Hindawi

Research Article

Mixed Maghemite/Hematite Iron Oxide Nanoparticles Synthesis for Lead and Arsenic Removal from Aqueous Solution

Koua Moro (iD), **Aimé Serge Ello** (iD), **Konan Roger Koffi** (iD), **and N'goran Séverin Eroi** (iD)

Laboratoire de Constitution et Réaction de la Matière, Université Felix Houphouët-Boigny, 22 bp 582, Abidjan 22, Côte d'Ivoire

Correspondence should be addressed to Aimé Serge Ello; elloserge@gmail.com

This work focused on the synthesis of iron oxide nanoparticles by the coprecipitation method with three basic solutions, namely, NH_4OH, KOH, and $NaOH$. The synthesized iron oxides were characterized by various techniques such as XRD, MET, BET, and a SQUID magnetometer. The results showed nanosized particles of 13.2, 9.17, and 8.42 nm and different phases associated to maghemite and maghemite/hematite. The surface areas were 113, 94, and 84 m^2/g and the magnetization strength were 58, 61, and 75 emu/g to iron oxides synthesized with $NaOH$, KOH, and NH_4OH, respectively. The magnetic iron oxides obtained using $NaOH$ were more efficient in the removal of lead and arsenic by adsorption than iron oxides obtained with KOH and NH_4OH. However, the magnetic strength decreases using $NaOH$ and KOH. The highest adsorption capacities attained for lead and arsenic removal were 16.6 and 14 mg/g, respectively, using $NaOH$-based iron oxides.

1. Introduction

Heavy metals constitute an important source of water pollution. In developing countries, water contaminated with heavy metals is caused by the excessive use of pesticides, chemical fertilizers in agriculture, and rapid industrialization. According to the World Health Organization (WHO), the toxicity of heavy metal pollution such as lead (Pb) and arsenic (As) affects not only human health but also our ecosystem [1]. Many countries have restricted levels of As and Pb in the water supply due to their harmful effects [1, 2]. The contaminated water needs to be treated and thus many researchers are interested in developing effective methods for contaminated water treatment. Several conventional physicochemical methods [3], including membrane filtration [4], chemical oxidation [5], chemical precipitation [6], ion exchange [7], coagulation [8], flocculation [9], and adsorption [10, 11], were applied for the treatment of heavy metals containing wastewater. Among these techniques, adsorption is considered as one of the most effective, fast, and simple operations for the efficient removal of heavy metals from aqueous solution. Recently, many researchers have focused on iron oxide magnetic nanoparticles as adsorbents because they exhibited high adsorption [12] and

provided feasibility for separation from aqueous media by using low magnetic field gradients. It was shown that an ideal magnetic sorbent should have the following advantages: (i) strong magnetism to achieve fast magnetic separation; (ii) good dispersion, so as to improve the adsorption/desorption kinetics; (iii) large specific surface area, suitable porosity, (iv) good stability, and (v) environmentally friendly. The use of iron-based nanomaterials allows easy separation using a magnetic field, but also increases the adsorption capacity. Therefore, magnetic particles can be a very good option for the adsorption of various metal ions [3]. The goal of this work is to highlight the contribution of iron oxide nanomaterials particles sizes and porosity on the adsorption process by varying only the magnetization strength of iron oxide particles. The adsorption of metal ions by only magnetic iron oxide particles is not often well studied. Different magnetic iron oxides were synthesized and tested for the removal of arsenic and lead, which are highly toxic pollutants.

2. Material and Methods

2.1. Synthesis. Iron oxide nanoparticles were synthesized by the coprecipitation method using an aqueous solution of Fe^{2+}

and Fe^{3+} with the stoichiometric ratio of $1:2$. The synthesis was done according to the following operating procedure: a mixture of 50 ml of Fe^{2+} and Fe^{3+} previously prepared with adding in 50 ml of deionized water, 1.41 and 2.76 g of $FeSO_4 \cdot 7H_2O$, and $FeCl_3 \cdot 6H_2O$, respectively. One hundred and eighty milliliter of deionized water was added by stirring to finally obtain 300 ml. Different amounts corresponding to 4 M concentration solutions of ammonium hydroxide (NH_4OH), sodium hydroxide (NaOH), and potassium hydroxide (KOH) were added dropwise while stirring. The black precipitates obtained between pH 10 and 12 were recovered, washed several times with deionized water until the pH was reduced to pH 7, and then dried at 70°C overnight. The samples were denoted, respectively, as IO-K, IO-Na, and IO-NH, where IO indicates iron oxide and K, Na, and NH indicate the basic solutions KOH, NaOH and NH_4OH used, respectively to synthesize iron oxide nanoparticles.

2.2. Characterization.

XRD was employed for analyzing the phase of the synthesized iron oxide nanomaterials. The XRD patterns were obtained using a Bruker D8 powder (XRD) instrument employing CuKα radiation ($\lambda = 1.5418$ Å). The iron oxide nanoparticles were further characterized using a transmission electron microscopy (TEM) instrument, using JOEL JEM-2100F model with a 200 keV. Nitrogen gas adsorption measurements were performed at −196°C by using a Micromeritics TriStar II plus instrument. Before adsorption measurements, all samples were outgassed at 200°C for at least 2 hr. The Brunauer–Emmett–Teller (BET) surface area was calculated from nitrogen adsorption isotherms in the relative pressure (p/p_0) range of 0.05–0.20. The total pore volume was estimated from the amount adsorbed at a relative pressure of 0.98. The pore size distributions (PSDs) were calculated from the adsorption branches of the isotherms by using the Barrett–Joyner–Halenda (BJH) method. For magnetic measurements, a vibrating sample magnetometer (VSM, Lakeshore, model 7400 series) was used at room temperature. The magnetic response of the iron oxide nanoparticles was also studied using a squid magnetometer (MPMS, Evercool, 7T Squid instrument supplied by Quantum Design). The neutral charge of the iron oxide synthesized surfaces was verified by point of zero charge (PZC). For this method, 0.1 g of iron oxide nanoparticles was added in 20 ml of deionized water under nine different initial pH conditions (from 2 to 11) and after 48 hr at 25°C, the pH was measured again. The pH-PZC corresponds to the range in which the final pH_f remains more constant at the different initial pH_i applied.

2.3. Heavy Metals Adsorption Experiments.

To measure the removal of heavy metals by the synthesized iron oxide nanoparticles, batch adsorption experiments were conducted by mixing 0.1 g of iron oxide with 25 ml of lead solutions and 50 ml of arsenic solutions at room temperature. Metal solutions of 5–50 mg/L were prepared by dissolving $Pb(NO_3)_2$ and $AsNaO_2$ in deionized water and adjusted the pH to 6.7 and 8 corresponding to the optimum pH (maximal adsorption conditions of lead and arsenic) for lead and arsenic metal ions, respectively. The iron oxide nanoparticles were added in each solutions, shaken in a mechanical shaker at
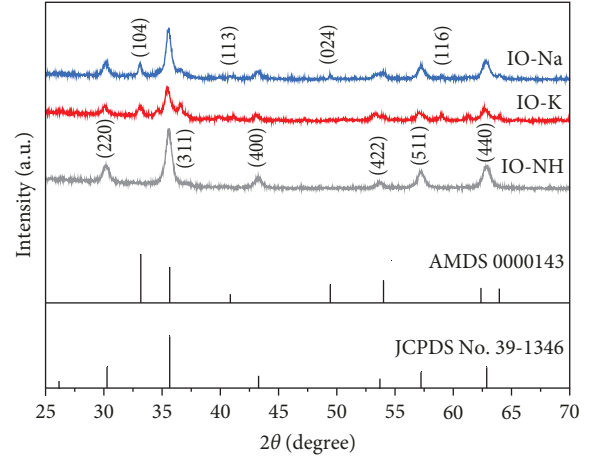
FIGURE 1: XRD patterns of IO-NH, IO-K, and IO-Na iron oxides.

150 rpm for 24 hr to achieve equilibrium, and then filtered through a 0.45 μm syringe filter. The residual concentrations of lead or arsenic ions in the aqueous filtrated were measured using atomic absorption spectrophotometer (spectr AA20) to assess the heavy metal adsorption capacity. The amount of heavy metals adsorbed per unit weight of iron oxide nanoparticles (Q_e, mg/g) is calculated using the following equation:

$$Q_e = \frac{(C_0 - C_e)V}{m}, \tag{1}$$

where C_0 and C_e represent the initial and equilibrium concentrations (mg/L) of the metal ions (Pb^{2+} or As^{3+}) in the solution, V is the aqueous solution volume (L), and m is the mass (g) of the iron oxide materials. The adsorption isotherms of Pb^{2+} and As^{3+} ions on iron oxide nanomaterials were fitted to linear Langmuir and Freundlich models, which are the most frequently used models for describing sorption isotherms. The Langmuir isotherm model is defined as Equation (2) [13], while the Freundlich isotherm model is given in Equation (3) [14]:

$$Q_e = \frac{abC_e}{1 + bC_e}, \tag{2}$$

$$\log Q_e = \frac{\log C_e}{n} + \log k, \tag{3}$$

where Q_e is the mass of metals adsorbed per mass of iron oxide (mg/g) at equilibrium, while C_e represents the equilibrium concentration (mg/L) of the metals. The Langmuir constants are a and b referred to the adsorption capacity and adsorption rate, respectively. The adsorption constants for the Freundlich model are k and n.

3. Results and Discussion

3.1. Characterization.

XRD patterns of synthesized iron oxide nanoparticles are shown in Figure 1. IO-NH sample shows intense peaks attributed to maghemite at $2\theta = 30.24°$,
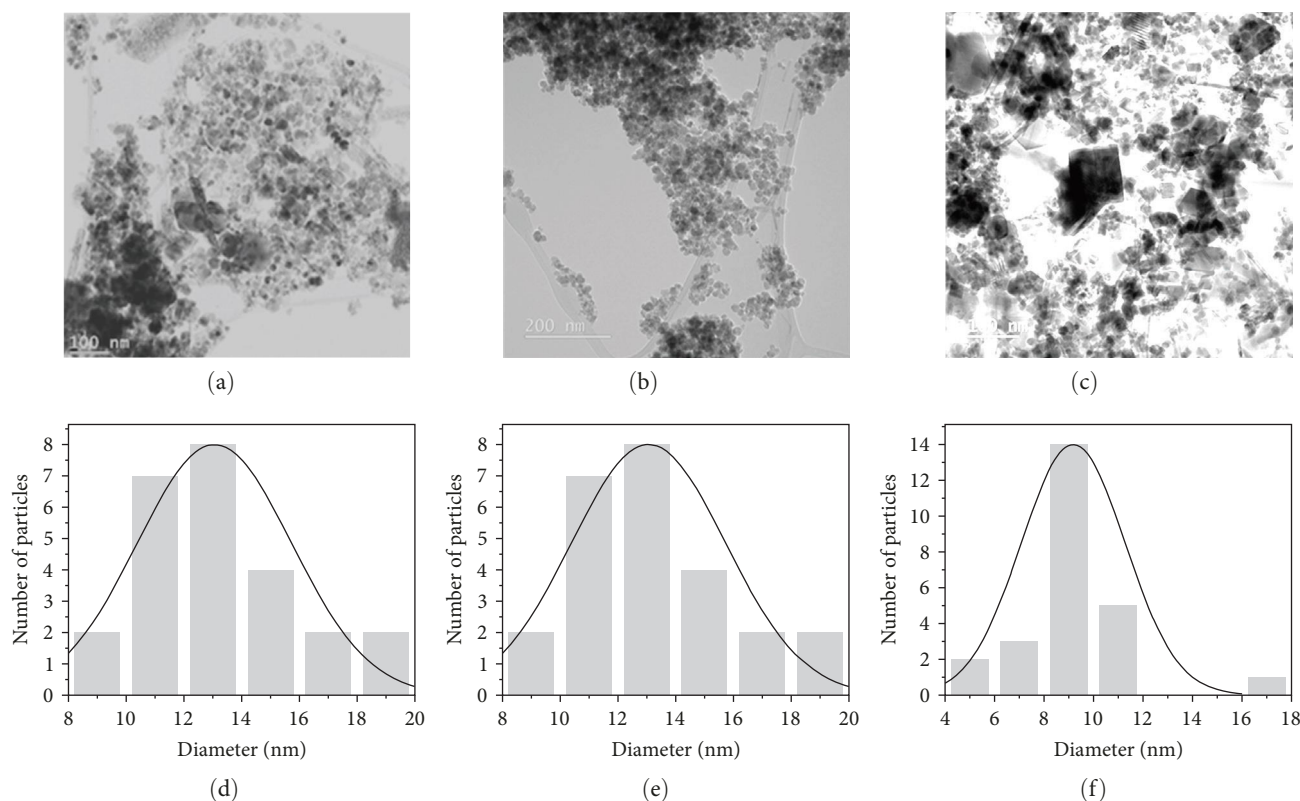
FIGURE 2: TEM images (a–c) for the synthesized iron oxides IO-NH, IO-K, and IO-Na, respectively, and particle size distribution, (d–f) for the synthesized iron oxides IO-NH, IO-K, and IO-Na, respectively.

35.63°, 43.28°, 53.73°, 57.27°, and 62.92° corresponding to the (220), (311), (400), (422), (511), and (440) family of planes, respectively, in agreement with JCPDS No. 00-039-1346. The maghemite crystalline structure was also observed using NH_4OH as basic solution [15]. The diffraction pattern corresponding to the samples IO-K and IO-Na exhibited same peaks associated to mixture of maghemite/hematite phase. The additional hematite phase is shown by the additional peaks at $2\theta = 33.15$, 40.86, 49.46, and 54.05 corresponding to the (104), (113), (024), and (116), respectively, identified in American Mineralogist Structure Database (AMSD) with the code 143 for hematite. The basic agents KOH and NaOH used for the synthesis of iron oxide showed the same crystalline phase comparatively to NH_4OH. The choice of the basic solution influenced the nucleation and the pH of the medium. The mechanism of iron oxide formation involved the step of hydroxylation of Fe^{3+} and Fe^{2+} ions. The subsequent addition of the basic solution at room temperature (pH < 3) led quasi instantaneously to a highly hydrated phase called ferrihydrite [16, 17]. Its transformation proceeded via different pathways depending on the acidity of the medium and resulted to different phases. The addition of strong bases such as KOH and NaOH, comparatively to the weak base NH_4OH, rapidly modified the acidity of the medium, thus the ferrihydrite was transformed into very small particles of hematite, followed by subsequent nucleation to produce maghemite structure. This transformation proceeded only by dehydration in situ and local rearrangement mechanism [16]. Hematite was therefore formed from ferrihydrite by an internal dehydration-

rearrangement mechanism. The addition of the weak base NH_4OH modified slowly the acidity of the medium and led to a progressive enlargement of the nucleation. The stoichiometric ratio of $Fe^{2+}/Fe^{3+} = 0.5$ is known to produce magnetite [17]. The transformation of magnetite into maghemite is due to the oxidation of magnetite by the air. The morphology of the samples IO-K, IO-Na, and IO-NH synthesized was studied as well as the particle sizes distribution was determined, as shown in Figure 2. The samples contain aggregates of nanoparticles whose dimensions were determined with TEM images and statistical analysis. The particle sizes of these samples were well described by a log-normal distribution (Figure 2(d)–2(f)) and showed values around 13.2, 9.17, and 8.42 nm for IO-NH, IO-K, and IO-Na, respectively. The change of iron oxide particle sizes was observed in previous work [18].

Figure 3 shows the nitrogen adsorption isotherms at −196°C and pore sizes distribution of iron oxide nanoparticles obtained with different basics solutions. Figure 3(a) shows the volume of adsorbed N_2 at a relative pressure (p/p_0) close to 0.1 increases slightly for all samples. However, the N_2 adsorption capacity at the relative pressure close to unity increases from 197 to 210 cm^3 STP/g. All the samples showed isotherms type II according to the IUPAC classification [19]. This type of isotherm is generally characteristic of nonporous materials. Figure 3(b) shows the diameter pores size and revealed a range mesoporous sizes; smaller diameter (<10 nm) and large diameter (>10 nm). We attributed these to the intraparticles porosity. As we showed above, the strong bases KOH and NaOH induce small particle size leading to very small intra-particles

(a)

(b)
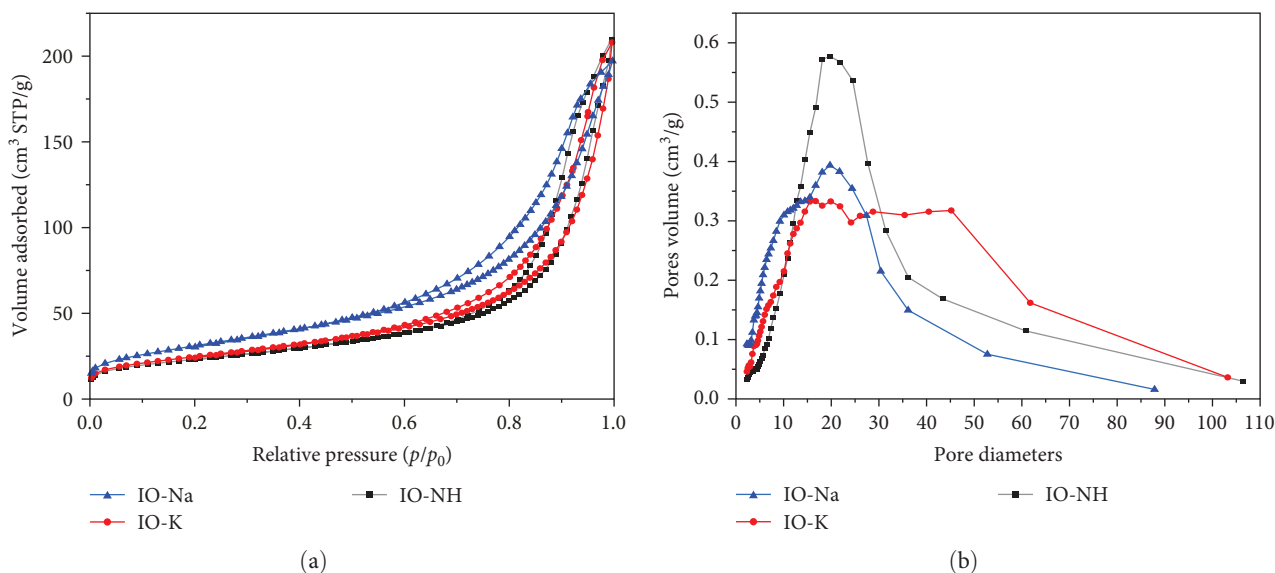
FIGURE 3: (a) Nitrogen adsorption–desorption isotherms at $-196°C$ and (b) pore size distribution for synthesized iron oxides IO-NH, IO-K, and IO-Na.
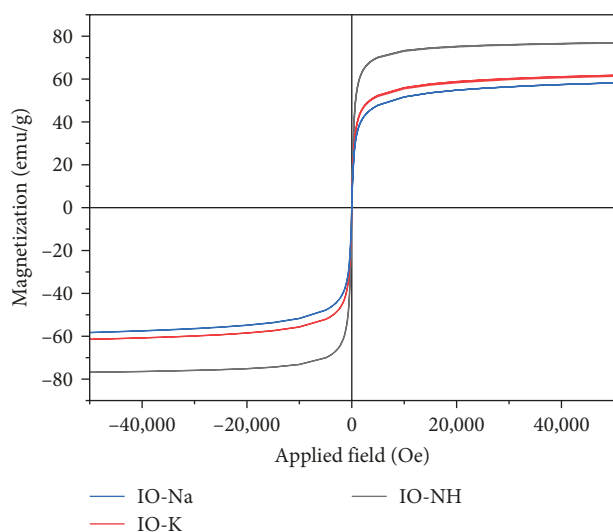
FIGURE 4: Magnetic hysteresis loops of the samples IO-NH, IO-K, and IO-Na at 27°C.

porosity ($d < 10$ nm) then the subsequent enlargement of the nucleation leads to large size with larger intraparticles porosity. The use of the weak base NH_4OH generated larger particles with wider intraparticles porosity, in addition to the contribution of the evaporation of ammonia. The surface areas obtained were 113, 94, and 84 m^2/g for IO-Na, IO-K, and IO-NH samples, respectively, according to the size of particles obtained.

The magnetic properties of the synthesized iron oxide nanoparticles were evaluated using a vibrating sample magnetometer (VSM) to investigate the saturation magnetization of iron oxide nanoparticles. Figure 4 shows a magnetization curve and determines the relationship between magnetization strength and external magnetic field intensity. The measurements were carried out at room temperature. Figure 4

shows the hysteresis-free magnetization curve indicating that all the samples are superparamagnetic. The use of different basic solutions for the synthesis of magnetic iron oxides had no effect on superparamagnetic feature of the particles obtained or do not destroy the superparamagnetism. The stationary point of the magnetization curve is the saturation magnetization strength and Figure 4 reveals that the magnetization strength are 58, 61, and 75 emu/g for the samples IO-Na, IO-K, and IO-NH, respectively. We observed that for the small particle sizes, magnetization strength is low contrary to large particles. In fact, the increase of magnetization increased the aggregation of particles. This effect has been frequently reported. The basic solutions caused difference in the H–M plot because of the particles size generated. These results indicated that iron-based materials resulting from NH_4OH as basic solution can be recovered easily with magnetic field than those from NaOH and KOH as basic solutions.

3.2. Heavy Metal Removal.
Figure 5 shows the heavy metals removal capacities of lead and arsenic on the three iron oxides synthesized. The capacities were 11.2, 13.1, and 16.6 mg/g of lead on IO-NH, IO-K, and IO-Na, samples respectively while those of arsenic were 8, 13, and 14 mg/g, respectively. The sample IO-Na showed the highest removal capacity for both heavy metals even though the magnetization strength is the lowest. As shown in Figure 3, the surface area of IO-Na is high comparatively to IO-NH and IO-K samples. It was demonstrated that the removal of heavy metal depends also on the size of iron oxide particles [20]. The amount of heavy metal adsorption removal increased with decreasing particle size due to less aggregation and more sites exposed to adsorption [20]. We observed in TEM the smallest particles in IO-Na, less aggregation than IO-NH, IO-K samples in agreement with its high adsorption capacity. The low magnetization strength of IO-Na sample had no effect on the adsorption capacity. The adsorption process is not governed by the magnetic structure.
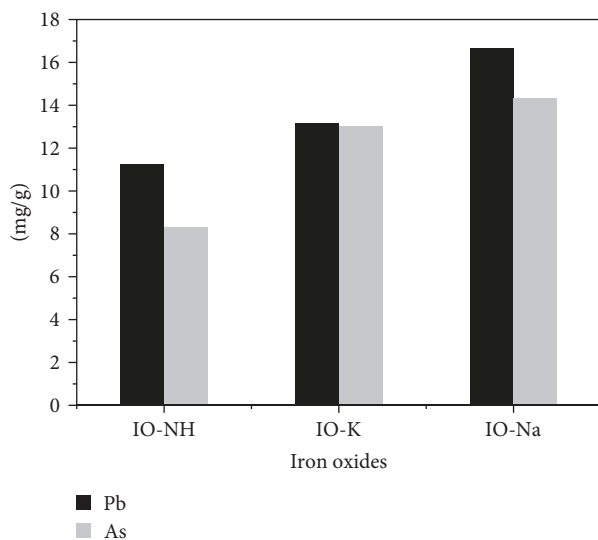
FIGURE 5: Heavy metals removal capacities of synthesized iron oxides at optimum pH 6.7 and 8 for lead and arsenic, respectively, with initial concentrations of 10 mg/L and mass of iron oxides = 0.1 g.
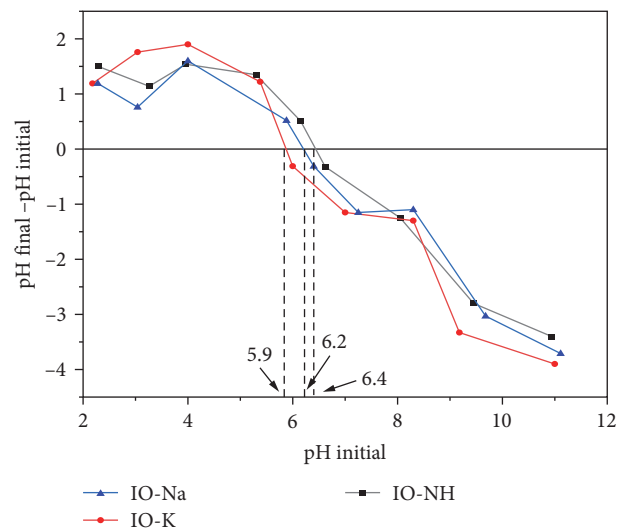
FIGURE 6: Point of zero charge of the samples IO-NH, IO-K, and IO-Na, mass of iron oxides = 0.1 g, initial concentrations of 10 mg/L.

TABLE 1: Comparison of heavy metal adsorption capacities of various iron oxide materials.

Heavy metal	Iron oxide	Q_e (mg/g)	References
	Fe_2O_3	36	[3]
	Magnetite	9.8	[23]
Pb	Iron oxide tea-waste	18.83	[24]
	Iron oxide–silica	16.4	[25]
	IO-Na	16.64	This study
	Flower-like iron oxide	5.5	[26]
	Hydrous iron oxide	8	[27]
As	Magnetite–maghemite	3.6	[28]
	Magnetite	0.99	[29]
	IO-Na	14.33	This study

The highest heavy metal adsorption capability of IO-Na sample can be attributed also to the small intraparticles porosity size observed (<10 nm) in IO-Na sample comparatively to IO-NH, IO-K. Adsorption is known to be favorable in very small pore size [21]. The addition effect is the electrostatic attraction between the iron oxide surface and the charge of metal ion. Figure 6 shows the PZC corresponding to the value of pH at which the charge detected on iron oxide particles surface becomes neutral. The PZC is helpful for the evaluation of charges on the surface [22]. PZC was found to be 5.9, 6.2, and 6.4 for IO-K, IO-Na, and IO-NH, respectively. At the optimal pH of this study (pH 6 and 8), all the iron oxides had negative charge (PZC < pH optimal), while lead (Pb) in cationic form and arsenic (As) in anionic form. The attraction of the opposite charges was an additional contribution to the sample intraparticle porosity to increase adsorption efficiency. These two contributions provided favorable conditions for heavy metal adsorption.

The difference in adsorption capacity of metal ions is due to the ions speciation. The negative surface charge of IO-Na generated a strong electrostatic attraction for cationic lead than for arsenic in anion form. Nevertheless, the iron oxide nanoparticles synthesized showed considerably higher heavy metal adsorption capability than the other types of iron oxide materials previously reported in the literature in Table 1.

The advantage of iron oxide nanoparticles is that they can be quickly recovered from the water using an external magnetic field even iron oxide nanoparticles easily undergo aggregation in aqueous solution systems which leads to decrease their specific surface area and adsorption capacity.

3.3. Isotherms. The heavy metals adsorption isotherms were simulated with the widely used Langmuir and Freundlich equations, and the corresponding parameters are summarized in Table 2, while the data are plotted in Figure 7. Adsorption isotherms of Pb (Figure 7(a)) and As (Figure 7(b)) on the sample IO-NH were better fitted with the Langmuir model, with a coefficient values of 0.97, 0.99 than the Freundlich model which showed values of 0.90 and 0.92. For the sample IO-K, Langmuir model was more suitable than the Freundlich model, although the difference in the coefficient values was very significant. In the case the sample IO-Na, the resulting

TABLE 2: The isotherm fitting parameters of different models of Pb and As adsorption on iron oxides; IO-NH, IO-K, and IO-NH.

	Heavy metal	Langmuir isotherm			Freundlich isotherm		
		a	b	R^2	k	n	R^2
IO-NH	Pb	12.58	1.36	0.99	5.94	2.65	0.90
	As	10.28	0.25	0.95	1.54	1.51	0.92
IO-K	Pb	15.45	1.11	0.96	6.01	2.05	0.83
	As	14.32	0.53	0.97	4.24	2.35	0.82
IO-Na	Pb	18.37	1.61	0.98	9.17	2.79	0.84
	As	16.05	0.50	0.97	4.67	2.33	0.86
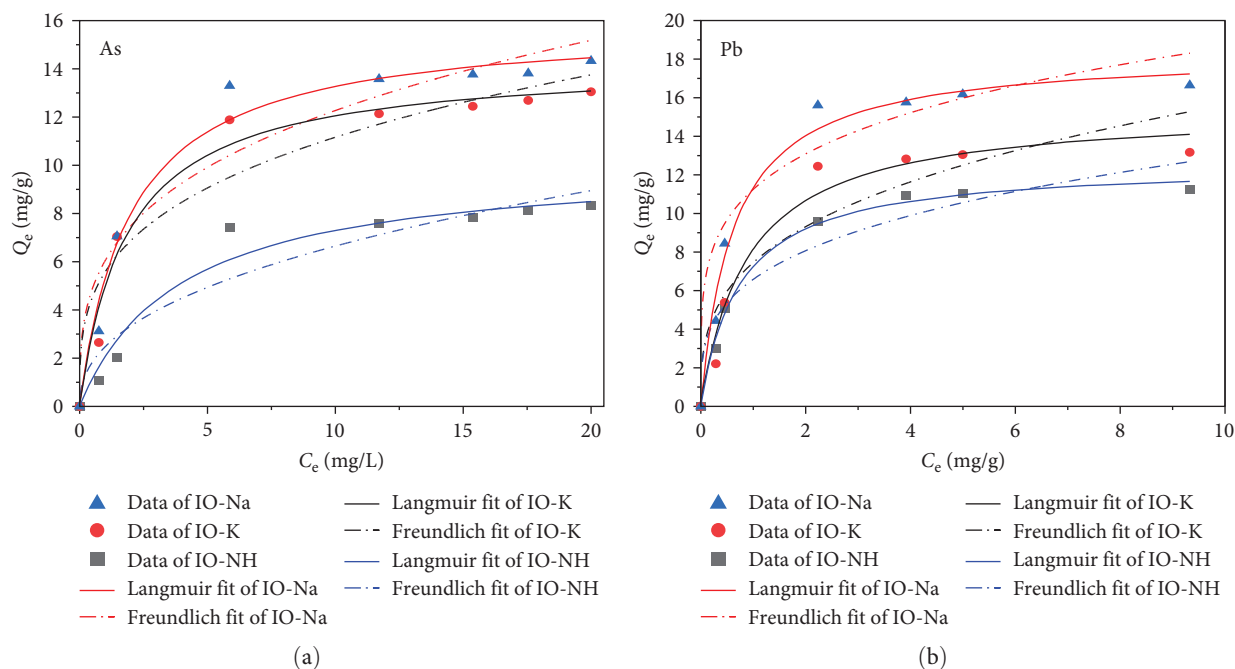
FIGURE 7: Adsorption isotherms fitting curves of (a) As on IO-NH, IO-K, and IO-NH according to models Langmuir and Freundlich models, (b) Pb on IO-NH, IO-K, and IO-NH according to models Langmuir and Freundlich models at pH = 8, initial concentration of 10 mg/L, mass of 0.1 g.

correlation coefficients also showed that Langmuir model was better fitted than Freundlich model. Previous works have shown the Langmuir model as a suitable isotherm reflecting adsorption of heavy metal such Pb and As [30, 31].

Renewability and reusability were important factors for an adsorbent. Thus, NaOH solution was used for the regeneration of the used adsorbents. A near-complete desorption of heavy metals from iron oxide particles by NaOH solution was occurred immediately. The adsorption stability of the iron oxide nanoparticles was investigated for the reusability tests, as shown in Figure 8. It was observed that adsorption efficiency of Pb by regenerated iron oxide adsorbents decreased after four cycles (i.e., 90.5% to 74.1%, 92.4% to 70.8%, and 95.9% to 70.3%) for IO-NH, IO-K, and IO-Na, respectively. The adsorption efficiency of As by regenerated adsorbents also decreased after four cycles (i.e., 90.2 to 79.2, 90.3 to 77, and 91.2 to 75) for IO-NH, IO-K, and IO-Na, respectively. The regenerated adsorbents showed the excellent reusability and stability

and the potential use to treatment of wastewater containing heavy metals.

4. Conclusion

Magnetic iron oxides were easily synthesized with different basic solution (NH₄OH, NaOH, KOH), and their properties were investigated using various characterization techniques. All the iron oxides obtained were superparamagnetic and in nanosize. Iron oxide synthesized from NaOH exhibited the highest adsorption of lead and arsenic because of high surface area, intraparticles porosity, and very high electrostatic attraction. Iron oxide synthesized from NH₄OH showed high magnetization strength but the magnetic properties had no effect on the adsorption process. The adsorption process was in agreement with Langmuir isotherm comparatively to Freundlich. The regenerated adsorbents showed the excellent reusability and stability. This work opens a way to the synthesis of new
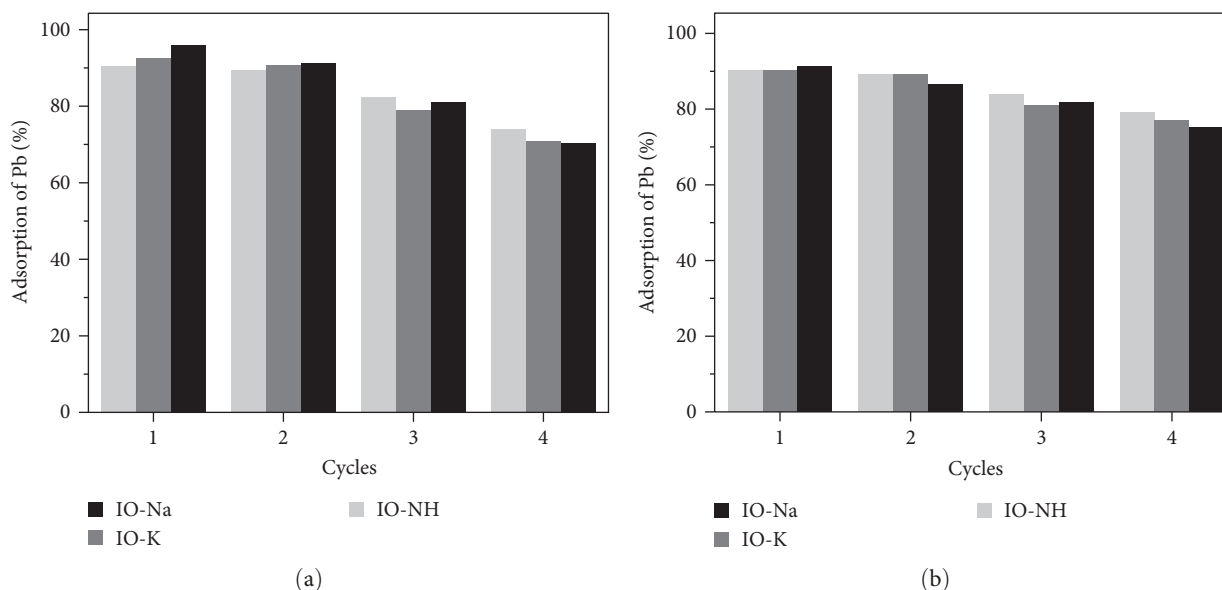
FIGURE 8: Reusability of iron oxides IO-Na, IO-K, and IO-Na for (a) Pb adsorption with initial concentration of 10 mg/L, mass of 0.1 g at pH = 6.7 and for (b) As adsorption with initial concentration of 10 mg/L, mass of 0.1 g at pH = 8.

materials-based iron oxides from NaOH to increase the adsorption of micropollutants including heavy metals.

Data Availability

Characterization and analytical data supporting the findings of this study are available from the corresponding author upon request. Table and figure data used to support the findings of this study are included within the article.

Conflicts of Interest

The authors declare that they have no conflicts of interest.

Acknowledgments

References

[1] E. Shaji, M. Santosh, K. V. Sarath, P. Prakash, V. Deepchand, and B. V. Divya, "Arsenic contamination of groundwater: a global synopsis with focus on the Indian peninsula," *Geoscience Frontiers*, vol. 12, no. 3, Article ID 101079, 2021.

[2] V. A. Beard and D. Mitlin, "Water access in global South cities: the challenges of intermittency and affordability," *World Development*, vol. 147, Article ID 105625, 2021.

[3] R. Bhateria and R. Singh, "A review on nanotechnological application of magnetic iron oxides for heavy metal removal," *Journal of Water Process Engineering*, vol. 31, Article ID 100845, 2019.

[4] T. S. Vo, M. M. Hossain, H. M. Jeong, and K. Kim, "Heavy metal removal applications using adsorptive membranes," *Nano Convergence*, vol. 7, Article ID 36, 2020.

[5] T. A. Saleh, M. Mustaqeem, and M. Khaled, "Water treatment technologies in removing heavy metal ions from wastewater: a review," *Environmental Nanotechnology, Monitoring & Management*, vol. 17, Article ID 100617, 2022.

[6] Q. Chen, Y. Yao, X. Li, J. Lu, J. Zhou, and Z. Huang, "Comparison of heavy metal removals from aqueous solutions by chemical precipitation and characteristics of precipitates," *Journal of Water Process Engineering*, vol. 26, pp. 289–300, 2018.

[7] A. Bashir, L. A. Malik, S. Ahad et al., "Removal of heavy metal ions from aqueous system by ion-exchange and biosorption methods," *Environmental Chemistry Letters*, vol. 17, pp. 729–754, 2019.

[8] D. Sakhi, Y. Rakhila, A. Elmchaouri, M. Abouri, S. Souabi, and A. Jada, "Optimization of coagulation flocculation process for the removal of heavy metals from real textile wastewater," in *Advanced Intelligent Systems for Sustainable Development (AI2SD'2018)*, M. Ezziyyani, Ed., vol. 913 of *Advances in Intelligent Systems and Computing*, pp. 257–266, Springer, Cham, 2019.

[9] Y. Sun, S. Zhou, S.-Y. Pan, S. Zhu, Y. Yu, and H. Zheng, "Performance evaluation and optimization of flocculation process for removing heavy metal," *Chemical Engineering Journal*, vol. 385, Article ID 123911, 2020.

[10] S. Rajendran, A. K. Priya, P. Senthil Kumar et al., "A critical and recent developments on adsorption technique for removal of heavy metals from wastewater—a review," *Chemosphere*, vol. 303, Part 2, Article ID 135146, 2022.

[11] C. Xu, Y. Feng, H. Li et al., "Adsorption of heavy metal ions by iron tailings: behavior, mechanism, evaluation and new perspectives," *Journal of Cleaner Production*, vol. 344, Article ID 131065, 2022.

[12] S. Lin, D. Lu, and Z. Liu, "Removal of arsenic contaminants with magnetic γ-Fe_2O_3 nanoparticles," *Chemical Engineering Journal*, vol. 211-212, pp. 46–52, 2012.

[13] X. Guo and J. Wang, "Comparison of linearization methods for modeling the Langmuir adsorption isotherm," *Journal of Molecular Liquids*, vol. 296, Article ID 111850, 2019.

[14] K. Walsh, S. Mayer, D. Rehmann, T. Hofmann, and K. Glas, "Equilibrium data and its analysis with the Freundlich model in the adsorption of arsenic(V) on granular ferric hydroxide,"

Separation and Purification Technology, vol. 243, Article ID 116704, 2020.

[15] C. P. Devatha and S. Shivani, "Novel application of maghemite nanoparticles coated bacteria for the removal of cadmium from aqueous solution," *Journal of Environmental Management*, vol. 258, Article ID 110038, 2020.

[16] J.-P. Jolivet, C. Chanéac, and E. Tronc, "Iron oxide chemistry. From molecular clusters to extended solid networks," *Chemical Communications*, no. 5, pp. 481–483, 2004.

[17] T. Ahn, J. H. Kim, H.-M. Yang, J. W. Lee, and J.-D. Kim, "Formation pathways of magnetite nanoparticles by coprecipitation method," *The Journal of Physical Chemistry C*, vol. 116, no. 10, pp. 6069–6076, 2012.

[18] M. C. Mascolo, Y. Pei, and T. A. Ring, "Room temperature co-precipitation synthesis of magnetite nanoparticles in a large pH window with different bases," *Materials*, vol. 6, no. 12, pp. 5549–5567, 2013.

[19] Z. Song, Y.-L. Ma, and C.-E. Li, "The residual tetracycline in pharmaceutical wastewater was effectively removed by using MnO_2/graphene nanocomposite," *Science of The Total Environment*, vol. 651, Part 1, pp. 580–590, 2019.

[20] A. Dey, M. Zubko, J. Kusz, V. R. Reddy, and A. Bhattacharjee, "Effect of reaction protocol on the nature and size of iron oxide nano particles obtained through solventless synthesis using iron(II)acetate: structural, magnetic and morphological studies," *SN Applied Sciences*, vol. 2, Article ID 193, 2020.

[21] A. S. Ello, L. K. C. de Souza, A. Trokourey, and M. Jaroniec, "Development of microporous carbons for CO_2 capture by KOH activation of African palm shells," *Journal of CO_2 Utilization*, vol. 2, pp. 35–38, 2013.

[22] S. Noreen, G. Mustafa, S. M. Ibrahim et al., "Iron oxide (Fe_2O_3) prepared via green route and adsorption efficiency evaluation for an anionic dye: kinetics, isotherms and thermodynamics studies," *Journal of Materials Research and Technology*, vol. 9, no. 3, pp. 4206–4217, 2020.

[23] X. Liang, G. Wei, J. Xiong et al., "Adsorption isotherm, mechanism, and geometry of Pb(II) on magnetites substituted with transition metals," *Chemical Geology*, vol. 470, pp. 132–140, 2017.

[24] M. Khanna, A. Mathur, A. K. Dubey et al., "Rapid removal of lead(II) ions from water using iron oxide–tea waste nanocomposite—a kinetic study," *IET Nanobiotechnology*, vol. 14, no. 4, pp. 275–280, 2020.

[25] L. P. Lingamdinne, J. R. Koduru, and R. Rao Karri, "Green synthesis of iron oxide nanoparticles for lead removal from aqueous solutions," *Key Engineering Materials*, vol. 805, pp. 122–127, 2019.

[26] A. R. Mahdavian and M. A.-S. Mirrahimi, "Efficient separation of heavy metal cations by anchoring polyacrylic acid on superparamagnetic magnetite nanoparticles through surface modification," *Chemical Engineering Journal*, vol. 159, no. 1–3, pp. 264–271, 2010.

[27] T. Pradeep and Anshup, "Noble metal nanoparticles for water purification: a critical review," *Thin Solid Films*, vol. 517, no. 24, pp. 6441–6478, 2009.

[28] S. R. Chowdhury and E. K. Yanful, "Arsenic and chromium removal by mixed magnetite–maghemite nanoparticles and the effect of phosphate on removal," *Journal of Environmental Management*, vol. 91, no. 11, pp. 2238–2247, 2010.

[29] W. Yang, A. T. Kan, W. Chen, and M. B. Tomson, "pH-dependent effect of zinc on arsenic adsorption to magnetite nanoparticles," *Water Research*, vol. 44, no. 19, pp. 5693–5701, 2010.

[30] M. E. Mejia-Santillan, N. Pariona, J. Bravo-C. et al., "Physical and arsenic adsorption properties of maghemite and magnetite sub-microparticles," *Journal of Magnetism and Magnetic Materials*, vol. 451, pp. 594–601, 2018.

[31] M. A. Ahmed, S. M. Ali, S. I. El-Dek, and A. Galal, "Magnetite–hematite nanoparticles prepared by green methods for heavy metal ions removal from water," *Materials Science and Engineering: B*, vol. 178, no. 10, pp. 744–751, 2013.